Behavior of the mass transfer coefficient during the MADE-2 experiment: New insights

Jianyong Guan,[1] Fred J. Molz,[2] Quanlin Zhou,[3] Hui Hai Liu,[3] and Chunmiao Zheng[4]

Received 16 April 2007; revised 7 August 2007; accepted 4 October 2007; published 19 February 2008.

[1] Using a dual-porosity transport model, a more complete analysis of the MADE-2 experiment, a natural gradient tracer (tritium) test, is presented. Results show that a first-order, mass transfer rate coefficient is scale-dependent and decreasing with experiment duration. This is in agreement with previous studies and predictions. Factors contributing to the scale-dependency are errors or approximations in boundary conditions, hydraulic conductivity (K) measurements and interpolations, mass transfer rate expressions and conceptual errors in model development. In order to formulate a self-consistent, dual-porosity model, it was necessary to assume that the injected tracer was trapped hydraulically in the vicinity of the injection site. This was accomplished by lowering all K values near the injection site by a factor of 30, while holding all other K values, boundary conditions and parameters at their measured or estimated magnitudes. Resulting simulations, using the same scale-dependent mass transfer rate coefficient, were then able to reasonably match the movement of the center of mass, overall plume geometry and the anomalous mass recovery ratios observed at each snapshot. The dual-porosity model is conceptually simple, relatively easy to apply mathematically and it simulates differences in advection that are probably the root cause of dispersion in natural heterogeneous sediments. Also, a small more realistic amount of local hydrodynamic dispersion is not precluded.

Citation: Guan, J., F. J. Molz, Q. Zhou, H. H. Liu, and C. Zheng (2008), Behavior of the mass transfer coefficient during the MADE-2 experiment: New insights, *Water Resour. Res.*, *44*, W02423, doi:10.1029/2007WR006120.

1. Introduction

[2] Between 1986 and 1992, a series of well-known tracer tests were performed at a site located on the Columbus Air Force base near the town of Columbus, MS [*Boggs et al.*, 1992, 1993; *Adams and Gelhar*, 1992; *Rehfeldt et al.*, 1992; *Boggs and Adams*, 1992]. The MADE site was unique in that the aquifer hydraulic conductivity (K) was highly heterogeneous, and thus more typical, compared to aquifers employed in previous tracer tests [*Boggs et al.*, 1992]. The present analysis is applied to the MADE-2 natural gradient tracer test that employed tritium as the conservative tracer. As described by *Boggs et al.* [1993], the test took place in an unconfined fluvial aquifer using the observation and sampling well field that was constructed for the MADE-1 tracer test that employed bromide as the main tracer [*Boggs et al.*, 1992]. As the observed tritium plume developed and was sampled using multilevel sampling wells, it was observed to have a slowly moving center of mass, with a leading edge far down-gradient. This led several groups to conclude that Gaussian dispersion theory was not consistent with the transport process taking place in the MADE aquifer [*Berkowitz and Scher*, 1998; *Harvey and Gorelick*, 2000; *Feehley et al.*, 2000; *Benson et al.*, 2001; *Zheng and Gorelick*, 2003; *Liu et. al.*, 2004a]. Several hypotheses were proposed, but the one studied herein is based on conceptualizing the MADE aquifer as a dual-porosity system. While this concept dates back over 4 decades [*Warren and Root*, 1963; *Coats and Smith*, 1964], it has been generalized more recently [*Haggerty and Gorelick*, 1995], and the dual porosity version, which visualizes transport as taking place in a so-called mobile porosity (high K) with storage and mass transfer with an intertwined immobile porosity (very low K), has been applied at the MADE site as well as the Savannah River Site [*Feehley et al.*, 2000; *Flach et al.*, 2004]. In general the results have been positive, with the dual-porosity or dual-domain conceptualization being superior to the traditional macro-dispersion conceptualization. The main reason is that the dual porosity model simulates macro-dispersion as a differential advection process (portions of fluids moving at different velocities) rather than as a concentration-gradient-driven diffusion process. While far from perfect, the differential advection conceptualization is likely closer to reality [*Feehley et al.*, 2000; *Flach et al.*, 2004; *Liu et al.*, 2004a; *Molz et al.*, 2006].

[3] In the more general theory developed by *Haggerty and Gorelick* [1995], the heterogeneous porous medium is actually conceptualized as a multiporosity system. This is due to the fact that in reality there would probably be many different rates of mass transfer between intermingled

[1]Daniel B. Stephens & Associates, Inc., Albuquerque, New Mexico, USA.
[2]Department of Environmental Engineering and Earth Science, Clemson University, Anderson, South Carolina, USA.
[3]Earth Sciences Division, Lawrence Berkeley National Laboratory, University of California, Berkeley, California, USA.
[4]Department of Geological Sciences, University of Alabama, Tuscaloosa, Alabama, USA.

0043-1397/08/2007WR006120$09.00

Table 1. MADE-2 Tracer Test Parameters (After *Boggs et al.*, 1993)

Tracer	Tritium
Injection period	2-day
Injection volume	9.7m^3
Injection well	5 wells 1 m apart
Mean concentration	55,610 pCi/mL
Total injected activity	0.5387Ci
Snapshots	27, 132, 224, and 328 days

regions of the aquifer having different K values. Multiple porosities may also be needed to deal accurately with lower K zones having variable geometry and to accurately model diffusive mass transfer [*Haggerty and Gorelick*, 1995]. Thus the more general mass transfer equation would be given by:

$$(\theta_{im})_j \frac{(\partial C_{im})_j}{\partial t} = \beta_j \left[C_m - (C_{im})_j \right], \qquad \theta = \theta_m + \sum_{j=1}^{N} (\theta_{im})_j, \qquad j = 1, 2, \ldots, N \tag{1}$$

where C_m is the solute concentration in the mobile porosity, $(C_{im})_j$ is the concentration in the jth immobile porosity, θ is the total porosity, θ_m is the mobile porosity, $(\theta_{im})_j$ is the jth immobile porosity value, β_j is the jth mass transfer coefficient and N is the number of immobile porosities. In such a system, solute mass in immobile porosities with large mass transfer coefficients would equilibrate rapidly with mass in the mobile porosity, while low mass transfer porosities would take much longer. Such a hierarchy of mass transfer rates in heterogeneous sediments, as opposed to fractured rock, seems highly likely [*Haggerty and Gorelick*, 1995].

[4] In practical applications to groundwater, of which the authors are aware, only the dual porosity version (N = 1) of equation (1) has been applied. This is due to the resulting mathematical simplicity as well as the difficulty in identifying rigorous values for several β values. Thus the practical version of (1), and the version analyzed herein, may be written as:

$$\theta_{im} \frac{\partial C_{im}}{\partial t} = \beta [C_m - C_{im}], \quad \theta = \theta_m + \theta_{im} \tag{2}$$

To avoid potential confusion, we note that previous studies dealing with mass transfer processes at the MADE site often used slightly different notation from that employed here. For example, *Harvey and Gorelick* [2000] used α to represent $\beta/\theta_{\mathrm{im}}$, while β was used to represent $\theta_{\mathrm{im}}/\theta_{\mathrm{m}}$.

[5] If one agrees that multiple mass transfer rates actually occur in heterogeneous porous media, or that unknown concentration gradients are affecting mass transfer rates, then the single β value in equation (2) would have to be interpreted as an apparent mass transfer coefficient. Because of the actual varying rates taking place with their various equilibration times, one would expect β to be scale-dependent and probably decrease with time or travel distance, since large β values would dominate initially and then smaller values. This question was studied in detail by *Haggerty et al.* [2004], and they did find that in the vast majority of cases (316 experiments were analyzed) apparent β was scale-dependent and decreased with time or travel distance, which is opposite to the well-known scale-dependence observed with apparent dispersivity.

[6] The present study is motivated by the desire to better understand the results observed in the MADE-2 experiments and to perform a more detailed analysis of the scale-dependence of the apparent β throughout the entire experiment. Hopefully, this will further clarify the transfer mechanisms that took place during the MADE-2 experiment, identify possible measurement errors and further clarify some recent controversy over how the MADE-2 experiment should be simulated [*Barlebo et al.*, 2004; *Molz et al.*, 2006; *Hill et al.*, 2006].

2. Tritium Tracer Test

[7] Details concerning the MADE-2 tracer test may be found in the work of *Boggs et al.* [1992, 1993], and in several other publications [*Feehley*, 1999; *Feehley et al.*, 2000; *Guan*, 2006]. The experiment was conducted over a period of approximately 15 months, from June 1990 to September 1991. The study was initiated with a two-day pulse injection of 9.7 m^3 of tritium solution with a mean concentration of 55,610 pCi/ml through five wells spaced one meter apart in a linear array, with each injection well screened over a 0.6 m interval between elevations 57.5 and 58.1 m. The injected activity of tritium was equivalent to 0.5387 Ci. A total of four snapshots of the tracer plume at times of 27, 132, 224, and 328 days after injection were performed using multilevel sampling wells (328 wells with 20–30 sampling points per well, for over 6000 sampling points). A summary is given in Table 1.

[8] Longitudinal by vertical cross sections through the center of the tritium plume at 27, 132, 224, and 328 days are shown in Figure 1. The plume is very irregular and highly variable vertically due to a mean groundwater velocity field affected by high K trends along the plume travel path. The injection wells are located in regions of relatively low K (10^{-5} m/s). Approximately 20 m down-gradient from the source, the front of the tritium plume slowly discharges into sediments in the middle to upper part of the aquifer having hydraulic conductivities of 10^{-4} to 10^{-3} m/s. In other words, the observed plume generally follows the more permeable strata in the middle to upper sections of the aquifer once it gets into those strata. Late in the experiment, a small portion of the plume apparently exited the sampling zone, but at such low concentrations that no significant effect would have been observed on calculated mass balances.

[9] The plume travels a considerable distance from the injection area at 328 days after injection. However, the location with the maximum observed concentration of approximately 3800 pCi/ml is less than 6 m away from the injection location, which implies that something in the vicinity of the injection site is trapping the tracer, while allowing a small amount to leak out. (We will return to this observation later.) The plume is observed to spread downstream extensively at a low concentration of 5 pCi/ml (only 0.13% of the maximum observed concentration), with the leading edge moving much faster than the center of mass. On the basis of Figure 1, the front moves at the average

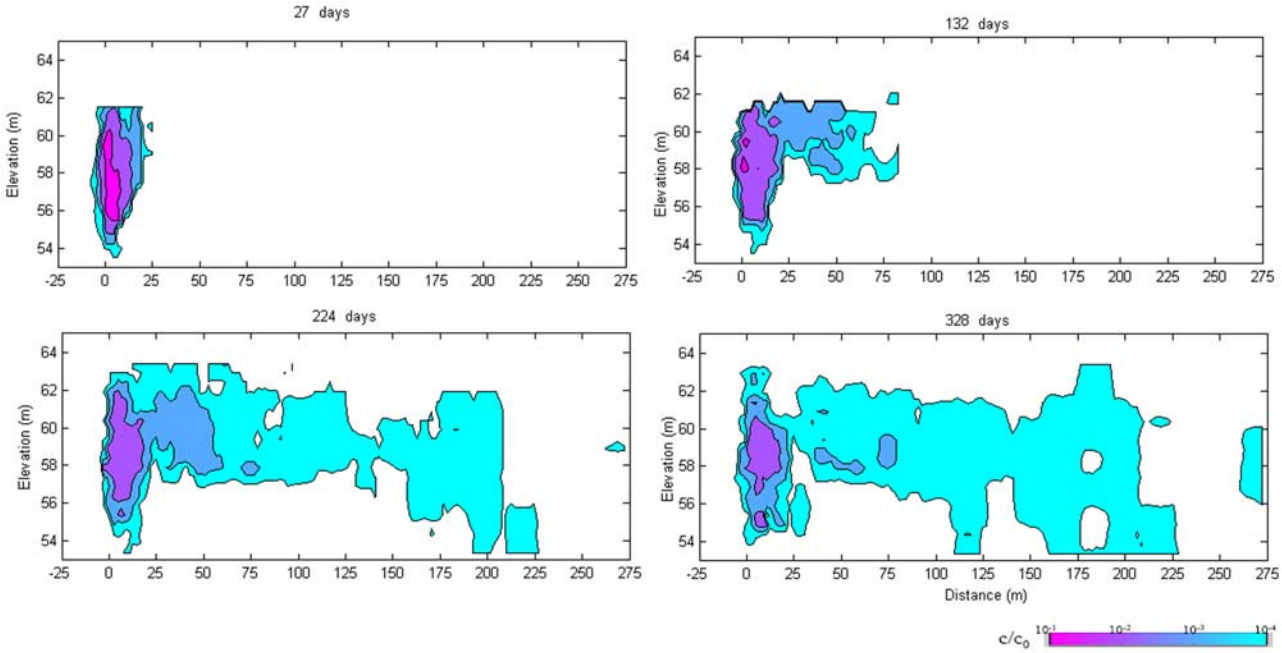

Figure 1. Centerline vertical cross-sections of the plume for each tracer concentration snapshot. The color code gives the ratio of the measured concentration to the injection concentration.

rates of 0.87 m/d, 0.56 m/d, and 1.55 m/d during the 27, 105, and 92 day periods preceding the first 3 snapshots. Of course, movement during the initial 27 day period was influenced by the injection process. (Our 3-D data are available upon request.)

3. Spatial Moment Analysis

[10] The spatial moments of the tritium concentration distribution are used to calculate the total tritium activity in the plume and the activity (mass) center for each snapshot. This is done assuming negligible tritium adsorption [*Harvey and Gorelick*, 2000] and a single porosity medium with the total measured porosity of 0.35, which is how the data were analyzed initially [*Boggs et al.*, 1993]. (Later, the dual porosity conceptualization will be used to explain any anomalies that may be observed.) The total plume mass is given by:

$$M_T = \int\int\int \theta C dx dy dz, \tag{3}$$

where C = tracer concentration, θ = total porosity of the porous medium, and the center of mass, x_c, y_c, z_c, along the three coordinate directions x, y, and z may be written as:

$$x_c = \frac{\int\int\int \theta c x dx dy dz}{M_T}$$
$$y_c = \frac{\int\int\int \theta c y dx dy dz}{M_T} \tag{4}$$
$$z_c = \frac{\int\int\int \theta c z dx dy dz}{M_T}$$

[11] The numerical implementation of the moment analysis is three-dimensional. Because the x and y positions are the same for each set of vertical samples, integration over the vertical (z direction) is performed at each sampler location assuming a linear variation between sampling points. With the z integration completed, the next step is to integrate over the x and y plane. In order to accomplish the horizontal integration, a primary triangular grid is constructed in the horizontal plane using the MLS as grid points, which is based on the approach of *Boggs et al.* [1993]. The horizontal region of each sub-domain is defined by constructing a secondary mesh with vertices at the centroids of triangles and at midpoints of their sides as shown in Figure 2. The surface areas A of the sub-domain associated with sampling point P is equal to the sum of one-third of the areas of all primary grid triangles sharing a vertex at P. Shown in Figure 3 is the triangular integration grid system constructed on a horizontal plane using MLS locations as grid points for the 27 day snapshot.

[12] The main results of the spatial moments analyses are shown in Figures 4 and 5, which give the relative mass recovery and center of mass as functions of time. Relative mass recovery is defined as $M_T/R_d M_0$, where M_0 is the initial mass (activity) injected, and R_d is the radioactive decay factor. This factor accounts for the fraction of tritium lost to radioactive decay since the start of the experiment. Using a half-life of 12.26 years [*Weast*, 1972], the decay factors for each snapshot are calculated to be 0.99, 0.98, 0.97 and 0.95, respectively. Complete mass recovery would result in $M_T/R_d M_0$ being 1 in the Figure 4 plot. However, calculations show too much mass recovery early in the experiment and too little late in the experiment. This phenomenon has been observed consistently during tracer experiments at the MADE site with both bromide and tritium [*Boggs et al.*, 1993]. The tritium mass recovery

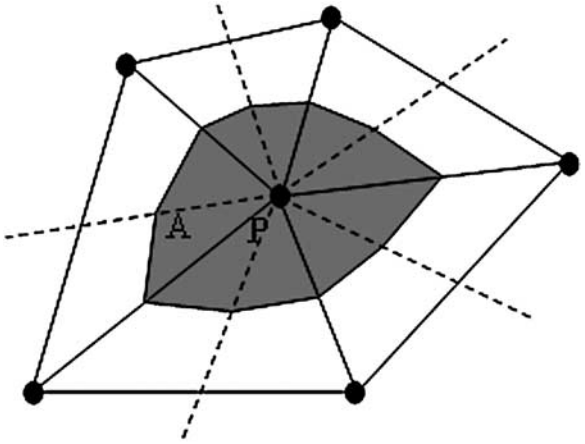

Figure 2. Tritium mass integration sub-domain associated with MLS point P (modified from *Boggs et al.*, 1993). Solid circles are sampling points; gray area between sampling points represent a triangular interpolation grid.

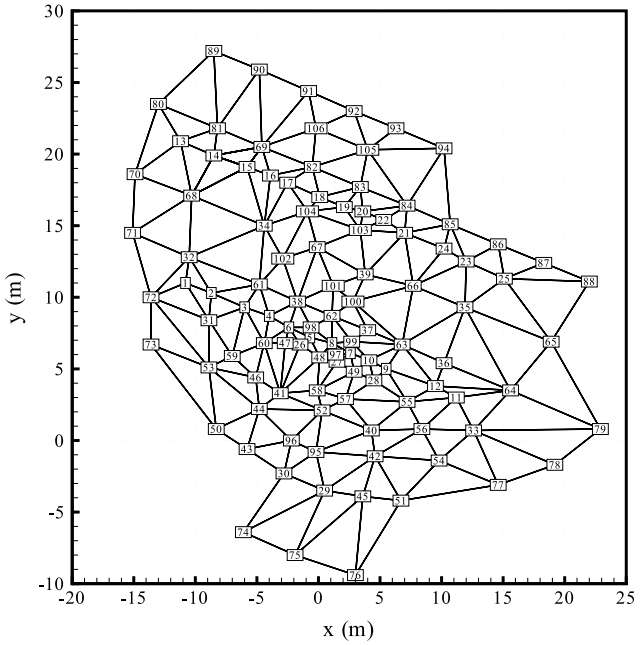

Figure 3. Plan view of the triangular integration system used to calculate spatial moments for the 27 day snapshot.

shows an abrupt decline between 27 and 132 days, but afterward the decrease followed a milder trend.

[13] Displayed in Figure 5 is the displacement of the mass center of the tracer plume for each snapshot as a function of time. On the basis of the distance and time duration, the mean mass center velocity for each time period is calculated. The mean velocity during the first 27 days is around 0.14 m/d, followed by a decrease to 0.04 m/d between 27 and 132 days. The mean velocity then accelerates to an average value of 0.42 m/d, followed by a decrease to 0.29 m/d. Several prominent quantities can affect the mean velocity, including evolving heterogeneity and mean head gradient changes due to seasonal recharge variations.

[14] Presented in Figures 4 and 5 are two key pieces of information for calibrating an apparent mass transfer coefficient in a dual porosity model. Mass in the mobile porosity moves relatively rapidly, so if the mass transfer coefficient is not too large, a small amount of mass can move far downgradient, as observed in the MADE experiments. Initially, most mass would be injected into the mobile porosity, and it would take some time to begin penetrating the immobile porosity. Thus only a portion of the total porosity would contain mass, and assuming that the concentrations measured by the multilevel samplers were uniform across both porosities would result in an over estimation early in the experiment, again as observed in the MADE experiments. Later in the experiment as equilibration between the two porosities occurred, the error would diminish. A self-consistent analysis would result in the same scale-dependent mass transfer coefficient for both scenarios. Ultimately, the mathematical model presented in the next section will be used to make such an analysis.

4. Mathematical Model

[15] The present mathematical model is based on quasi-steady state, 3-D flow in the MADE aquifer, along with transient, 3-D, mass transport using the dual-porosity advection-dispersion equation. The required equations are given by:

$$\frac{\partial}{\partial x}\left(K_x\frac{\partial h}{\partial x}\right)+\frac{\partial}{\partial y}\left(K_y\frac{\partial h}{\partial y}\right)+\frac{\partial}{\partial z}\left(K_z\frac{\partial h}{\partial z}\right)+q_s(x,y,z)=0 \quad \textit{Flow};$$

$$\theta_m\vec{v}=-K_x\frac{\partial h}{\partial x}\vec{i}\ -K_y\frac{\partial h}{\partial y}\vec{j}\ -K_z\frac{\partial h}{\partial z}\vec{k} \qquad \textit{Darcy's law};$$

$$\begin{aligned}\theta_m\frac{\partial C_m}{\partial t}+\theta_{im}\frac{\partial C_{im}}{\partial t}&=\frac{\partial}{\partial x}\left(\theta_m D_x\frac{\partial C_m}{\partial x}\right)+\frac{\partial}{\partial y}\left(\theta_m D_y\frac{\partial C_m}{\partial y}\right)\\&+\tfrac{\partial}{\partial z}\left(\theta_m D_z\tfrac{\partial C_m}{\partial z}\right)-\frac{\partial}{\partial x}(\theta_m v_x C_m)-\frac{\partial}{\partial y}(\theta_m v_y C_m)-\frac{\partial}{\partial z}(\theta_m v_z C_m)\\&+q_s C_s \qquad \textit{Transport};\end{aligned} \tag{5}$$

and $\theta_{im}\frac{\partial C_{im}}{\partial t}=\beta[C_m-C_{im}]$ *Mass exhange*.

[16] Variables in equation (5) are head "h", hydraulic conductivities in the x, y and z directions "K_x, K_y, and K_z ",

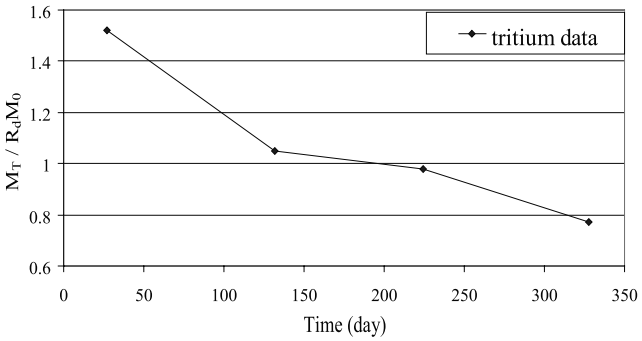

Figure 4. Temporal trends in relative mass fraction.

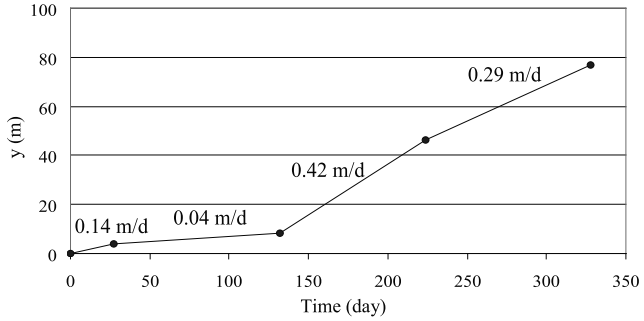

Figure 5. Temporal trends in the horizontal displacement of the center of mass in the longitudinal direction.

a source term "q_s" with source concentration "C_s", a seepage velocity vector "$\vec{v}$" with components "v_x, v_y, v_z", and dispersion coefficients D_x, D_y, and D_z. This partly coupled system of equations is solvable using MODFLOW [*McDonald and Harbaugh*, 1988] and MT3DMS [*Zheng and Wang*, 1999]. The procedure is to solve the flow equation to get the head "h" distribution, and use Darcy's law to obtain the velocity distribution. Velocity components then go into the transport equation, which is solved simultaneously with the mass exchange equation to simulate the evolution of the MADE tritium plume. In order to accomplish this, one must make use of measured and estimated quantities, including aquifer geometry, porosities, tracer injection rates, K values from borehole flowmeter tests, boundary conditions and recharge rates. A cartoon of the dual porosity concept is presented in Figure 6.

[17] The 3-D finite difference groundwater-flow model covers a 306 m by 110 m by 11 m volume that is subdivided into 181,300 grid cells (Figure 7). The model grid consists of 153 rows, 53 columns, and 22 layers. The horizontal spacing of each node is uniform throughout the model area, with spatial steps of 2 m. Node spacing in the z (vertical) direction is 0.5 m. East and west boundaries are no-flux normal to approximate flow lines, and the north and south boundaries are constant head along approximate head-contour lines. The constant head changes linearly in the vertical dimension between the two measured levels at the

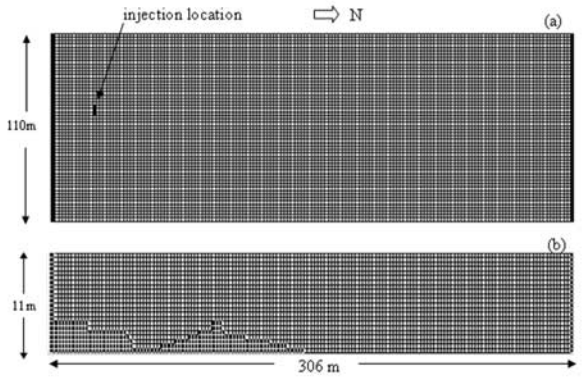

Figure 7. A plan view (a) and a y–z cross-sectional view (b) of the model grid system.

south and north ends of the domain. A no-flow boundary is specified at the bottom corresponding to an observed low permeability marine clay/sand unit.

[18] The top surface of the model is simulated as a free surface that receives recharge. A specific-recharge rate of 0.14 mm/d is used in all simulations [*Feehley et al.*, 2000]. This areal recharge is simulated using the Recharge Package (RCH) in MODFLOW.

[19] Although a steady flow model is used, it was observed that two distinct climatic periods existed during the MADE-2 study. This is illustrated in Figure 8, showing the mean head gradient across the MADE site, based on water level measurements in wells p61A and p53A. It is clear from Figure 8 that the first 6 months of the experiment were quite stable hydraulically, with a slightly decreasing hydraulic gradient. After that period, the average gradient increased significantly and became more variable. As shown in Table 2, we ended up dividing the experiment into three time periods, with average head gradients of 0.0029, 0.0023, and 0.0058. Thus three different steady state flow fields were applied in order to more realistically simulate the tritium transport process. As will be illustrated later, neglecting major variations results in anomalous scale-dependence of the calibrated mass transfer coefficient.

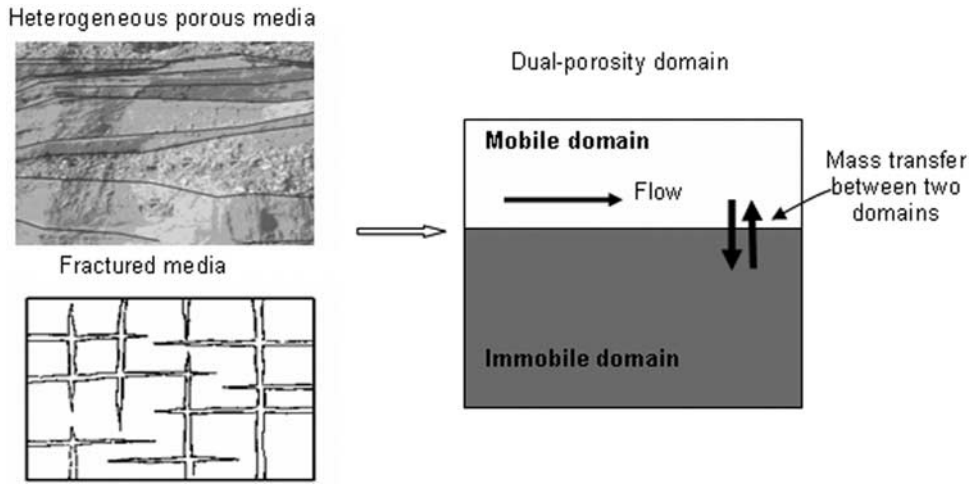

Figure 6. Two possible types of heterogeneity that could lead to use of a dual-porosity flow and transport model.

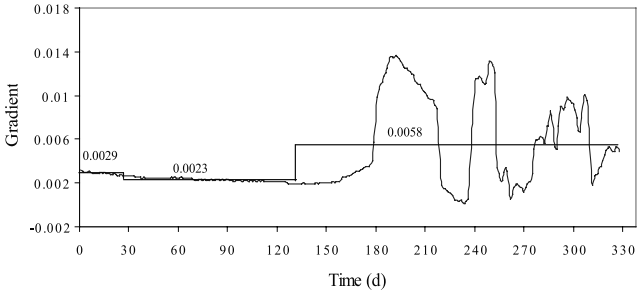

Figure 8. Water table gradient as a function of time between observation wells p61A and p53A, which span the sampling network in the mean flow direction.

[20] To accommodate tracer injection in the model, and to account for the varying mean gradient shown in Table 2, the flow field over 328 days is approximated by four steady state stress periods of 2, 25, 105, and 196 days. The tritium solution was injected into the wells at a uniform rate of 4.75 m^3/d.

[21] It is generally recognized that the heterogeneity of the aquifer hydraulic conductivity field controls the movement and dispersion of groundwater solutes. If hydraulic conductivities K could be measured everywhere in the flow system, the velocity field would be obtained accurately. In reality, K was observed at widely spaced locations compared to the grid size, even in the relatively detailed MADE experiment. Therefore values for hydraulic conductivity at model grid nodes without measurements are assigned by an interpolation algorithm which is essential for the application of solute transport models to practical problems.

[22] For flow simulation, all interpolation is performed on ln (K_h) (horizontal hydraulic conductivity) data and then transformed to K_h values. Values for ln (K_h) at grid nodes are interpolated using a fractional Brownian motion model, the same model utilized by *Feehley et al.* [2000]. A fractional Brownian motion (fBm) field is a correlated random field in which the variability is statistically self-affine at all scales [*Molz and Boman*, 1993; *Molz et al.*, 1997]. Such a model assumes that the increments of ln(K_h) are stationary, hence the interpolation of ln(K_h) rather than K_h. Vertical hydraulic conductivity (K_v) values are assumed to be proportional to K_h. On the basis of previous studies, an average K_v/K_h of 0.139 is used to compute nodal K_v values for the K field of the model [*Feehley et al.*, 2000].

5. Simulation of the Total Mass and Mass Center Location

[23] The transport parameters used in the model simulations are summarized in Table 3. The value for total porosity of 0.35 was estimated based on analyses of 84 soil cores collected from the MADE site [*Boggs et al.*, 1992]. Following *Feehley et al.* [2000], a longitudinal dispersivity of 1 m was selected, along with a ratio of the longitudinal to transverse dispersivity of 0.01, and a ratio of longitudinal to vertical dispersivity of 0.001. Thus the small dispersivity values did not play a significant role in the simulations.

Table 2. Variations of Head Gradient With Time

Region	1	2	3
Time Period	0∼27	27∼132	132∼328
Applied Head Gradient	0.0029	0.0023	0.0058

Table 3. Input Parameters for the Dual-Porosity Transport Model

Model	Dual-Porosity Mass Transfer
Dimension	3-D
K-field generating scheme	Fractal Brownian motion (fBm)
Hydraulic gradient	0.0029, 0.0023, 0.0058
Longitudinal dispersivity, m	1
Transverse dispersivity, m	0.01
Vertical dispersivity, m	0.001
Ratio of mobile to total porosities	1/8
Total porosity	0.35
Mass transfer rate coefficient (β), d^{-1}	Trial and error

[24] For the dual-porosity mass transfer model, we need to specify two additional parameters including the ratio of mobile to total porosities and the mass transfer rate coefficient. On the basis of a literature review devoted to MADE site studies, a mobile porosity of 1/8 of the total porosity was judged to produce the most consistent match between the observed and calculated plumes in previous studies [*Feehley et al.*, 2000; *Harvey and Gorelick*, 2000]. The best β values were selected by trial and error.

[25] There are several different considerations when calculating total mass using the dual-porosity model and comparing results to the MADE-2 data. There is (1) simulated total mass in the mobile porosity (M_m), (2) simulated total mass in the immobile porosity (M_{im}) and (3) simulated total mass in an assumed single porosity (M_s) using the concentration distribution in the mobile domain. As defined, M_s is comparable to the value for total mass obtained from concentration measurements during the MADE-2 experiment, since the mobile domain is preferentially sampled by the multilevel wells, and a single porosity medium was assumed initially by those performing the experiment [*Boggs et al.*, 1993]. These quantities are given by:

[26] 1. Mass in the mobile domain:

$$M_m = \int\int\int \theta_m c_m dxdydz \tag{6}$$

[27] 2. Mass in the immobile domain:

$$M_{im} = \int\int\int \theta_{im} c_{im} dxdydz \tag{7}$$

[28] 3. Mass in an assumed single porosity domain:

$$M_s = \int\int\int \theta c_m dxdydz \tag{8}$$

[29] We can also define the mass centers in the mobile and immobile porosities, as well as a mass center in an assumed single porosity using the concentration distribution in the mobile porosity. These three mass centers are given in equations (9) through (11).

Table 4. Comparison of Simulated Mass Center Locations With Those Calculated From the MADE-2 Data[a]

Snapshot Time (d)	27	132	224	328
Mass Center (m): (Data)	3.9	8.1	46.5	76.8
Mass Center (m): (Model)	3.65	9.42	45.23	77.92
	$\beta = 0.5\text{d}^{-1}$		$\beta = 0.002\text{d}^{-1}$	$\beta = 0.0005\text{d}^{-1}$

[a]The match was optimized by letting β decrease with travel distance.

[30] 1. Mass center in the mobile porosity:

$$x_{cm} = \frac{\int\int\int \theta_m c_m x dx dy dz}{M_m}$$
$$y_{cm} = \frac{\int\int\int \theta_m c_m y dx dy dz}{M_m} \quad (9)$$
$$z_{cm} = \frac{\int\int\int \theta_m c_m z dx dy dz}{M_m}$$

[31] 2. Mass center in the immobile porosity:

$$x_{cim} = \frac{\int\int\int \theta_{im} c_{im} x dx dy dz}{M_{im}}$$
$$y_{cim} = \frac{\int\int\int \theta_{im} c_{im} y dx dy dz}{M_{im}} \quad (10)$$
$$z_{cim} = \frac{\int\int\int \theta_{im} c_{im} z dx dy dz}{M_{im}}$$

[32] 3. Mass center in an assumed single porosity:

$$x_{cs} = \frac{\int\int\int \theta c_m x dx dy dz}{M_s}$$
$$y_{cs} = \frac{\int \theta c_m y dx dy dz}{M_s} \quad (11)$$
$$z_{cs} = \frac{\int\int\int \theta c_m z dx dy dz}{M_s}$$

[33] The required integrations in equations (6) through (11) must be performed numerically. This was done by using the relatively fine model grid (2 m by 2 m by 0.5 m volumes), multiplying each volume by the average of the activities at the 8 vertices and summing over the model domain.

6. Calibration of β to the Mass Center Location and Relative Mass Recovery

[34] In order to match the center of mass calculated from the MADE-2 data, it was necessary to decrease β with traveltime as expected. Multiple runs are required for adjusting the β values to fit the mass centers from the data at each snapshot. The procedure was to find a β value that resulted in a reasonable match for the mass center at the first snapshot, then find another β value that matched the second snapshot mass center, still another for the third, etc. The results are given in Table 4.

[35] One thing that stands out in these results is the huge value of β that is required to match the data during the first two snapshots, much larger than any values determined previously [*Feehley et al.*, 2000; *Flach et al.*, 2004]. This large value of β slows the advance of the plume initially. Without this retarding effect, the simulated mass center would have moved much further down-gradient than what was observed in the experiment.

[36] In order to check the self-consistency of the model so far, we simulated the mass recovery ratio assuming a single porosity medium and compared the results to the (assumed) single porosity ratio measured in the experiments. (As mentioned previously, we also corrected the data for radioactive decay during the 328 day experiment, although the corrections were relatively small.) The results shown in Figure 9 are not good for the early time period. The large value of β required to match the mass center results in rapid equilibrium between the mobile and immobile domains and no excess mass recovery. Since at equilibrium the mass concentration is the same in both domains, the simulated system behaves like a single porosity domain, and no apparent excess mass is found. The simulated mass recovery is near 100% for the first snapshot, while that from the experiment is about 153%. Thus the scale-dependent β function necessary to match the center of mass does not simultaneously reproduce the measured mass recovery ratio.

[37] The basic problem is that the simulated mass center is moving too rapidly given the hydraulic conductivity distribution utilized in the vicinity of the injection site, and slowing it down with tracer movement into the immobile domain requires an unrealistically large β value. So if

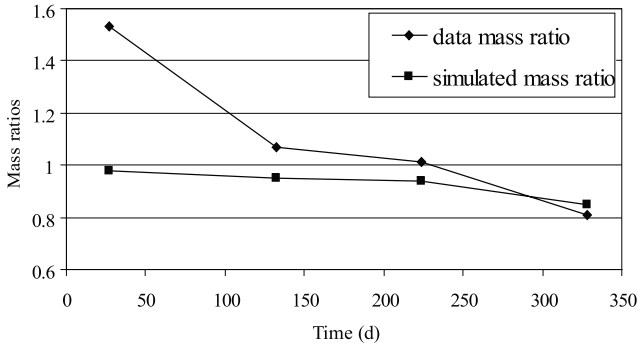

Figure 9. Plot of the ratio of the apparent mass recovery divided by the mass injected in the MADE-2 experiment (Data Mass Ratio) compared to the simulated mass recovery using the scale-dependent β shown in Table 4 and an assumed single porosity medium. The early fit is not good.

Table 5. Comparison of the Simulated Movement of the Center of Mass During the MADE-2 Experiment With That Resulting From the Data[a]

Snapshot Time (d)	27	132	224	328
Mass Center (m): (data)	3.9	8.1	46.5	76.8
Mass Center (m): (Model)	4.1	8.6	45.9	76.8
	$\beta = 0.004 d^{-1}$	$\beta = 0.002 d^{-1}$	$\beta = 0.00055 d^{-1}$	$\beta = 0.00012 d^{-1}$

[a]Permeability values near the source have been lowered by a factor of 30, and the 27 day (first snapshot) β value has been lowered by 2.1 orders of magnitude.

mass exchange is not the phenomenon retarding the mass center advance given the measured and interpolated K distribution, it must be unknown hydraulic properties of the aquifer. In fact, examination of the tracer distribution shown in Figure 1, and in other previous studies, suggests strongly that a large portion of the injected tracer is trapped near the source and leaking out of a limited area in roughly the top half of the vertical expanse of the near-source tracer spreading zone (elevations 58 m to 62 m in Figure 1). In the lower half of the near-source tracer spreading zone (elevations 54 m to 58 m), the tracer front is stopped at about 25 m after 27 days, and remains essentially fixed for the remainder of the experiment, an additional 301 days. Whatever is causing this entrapment, it is not resolved by the measured K distribution in the vicinity of the injection site.

[38] Previous simulations, not presented here, indicated that a mass transfer coefficient value of about 0.004 d^{-1} during the first 27 days of the experiment produced a mass balance ratio that agreed with the MADE-2 data. In order to simulate the effects of near-source entrapment, the measured K values in the region where the plume appears to become trapped (24 m by 15 m by 7 m in the x, y and z directions respectively) were ultimately lowered by a factor of 30. Other values and boundary conditions were kept as measured. As shown in Table 5 and Figure 10, the simulation now agrees quite well with the data, which was the main criterion for choosing the factor of 30. (Full justification for such a value will require additional field study.). The overall plume geometry is also simulated reasonably well with near-source trapping, as documented in Figure 11. Following the method developed by *Feehley et al.* [2000], the aquifer was divided into 6 equally spaced zones along the flow direction (width $\approx$ 50 m). In each zone, mass recovery during the experiment was calculated and compared to simulated mass recovery (Figure 11) for each snapshot, using an assumed single porosity aquifer.

[39] Shown in Figure 12 are semi-log plots of the scale-dependent mass transfer coefficients versus time, with and without trapping. The time variation with trapping is much smoother, and the values more reasonable when compared to previous studies [*Feehley et al.*, 2000; *Flach et al.*, 2004]. The *Feehley et al.* [2000] calibrated β value for the fBm interpolated K distribution for the last snapshot (328 days) was 0.0005, which is the same as our value without trapping. With trapping, our β value at 328 days becomes 0.00012, which is less by about a factor of 4. Thus there is a definite interplay between the K distribution used in a simulation and the resulting calibrated mass transfer coefficient, as already shown by *Feehley et al.* [2000]. In this sense, the scale-dependence is not unique.

[40] With trapping, the scale-dependent mass transfer coefficient varies with time in a near exponential manner. Only the 27 day value is slightly low, with the other three values falling approximately on a straight line. A rough exponential fit to the bottom curve in Figure 12 is: β (t) = 0.007exp (−0.0118t), where t is time in days. This result may be compared to those presented by *Haggerty et al.* [2004]. Their results, from many observations of scale-dependence, were summarized roughly by β/θ_{im} = 10/t, where t (called t_{exp} by *Haggerty et al.*, 2004) is the time since the start of the various experiments (tracer traveltime). For our immobile porosity of 0.306, this would yield β = 3.06/t. Actually fitting our results with trapping to an inverse time relationship yields approximately β = 0.41/t if the data point at 27 days is ignored, since that point does not fit the inverse-time relationship well. To fit well, β at 27 days would have to be 0.015 rather than 0.004, larger by a factor of 3.75. The 27-day β value also deviates the most from an exponential relationship with time, and is probably the data point most effected by ill-defined trapping in the injection point vicinity.

[41] In order to provide an additional feel for the scale-dependence of β, we kept all parameters for the case with trapping unchanged, but applied a single average head difference (0.0038) across the flow domain, instead of a difference derived from the 3 different average gradients listed in Table 2. The resulting calibrated β values and mass center positions are shown in Table 6. The first β value is increased by a factor of 2, the second value is increased by a factor of 3, the third is decreased by a factor of 2.75, and the

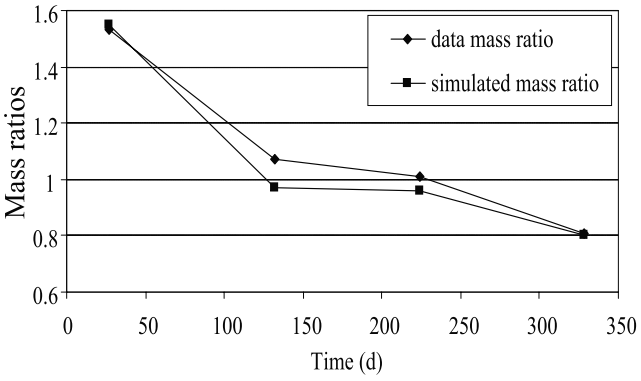

Figure 10. Simulated single porosity mass recovery ratio compared to the experimental mass recovery ratio for each snapshot. In order to simulate trapping, permeability values near the source have been lowered by a factor of 30, and the scale-dependent β values listed in Table 5 were utilized.

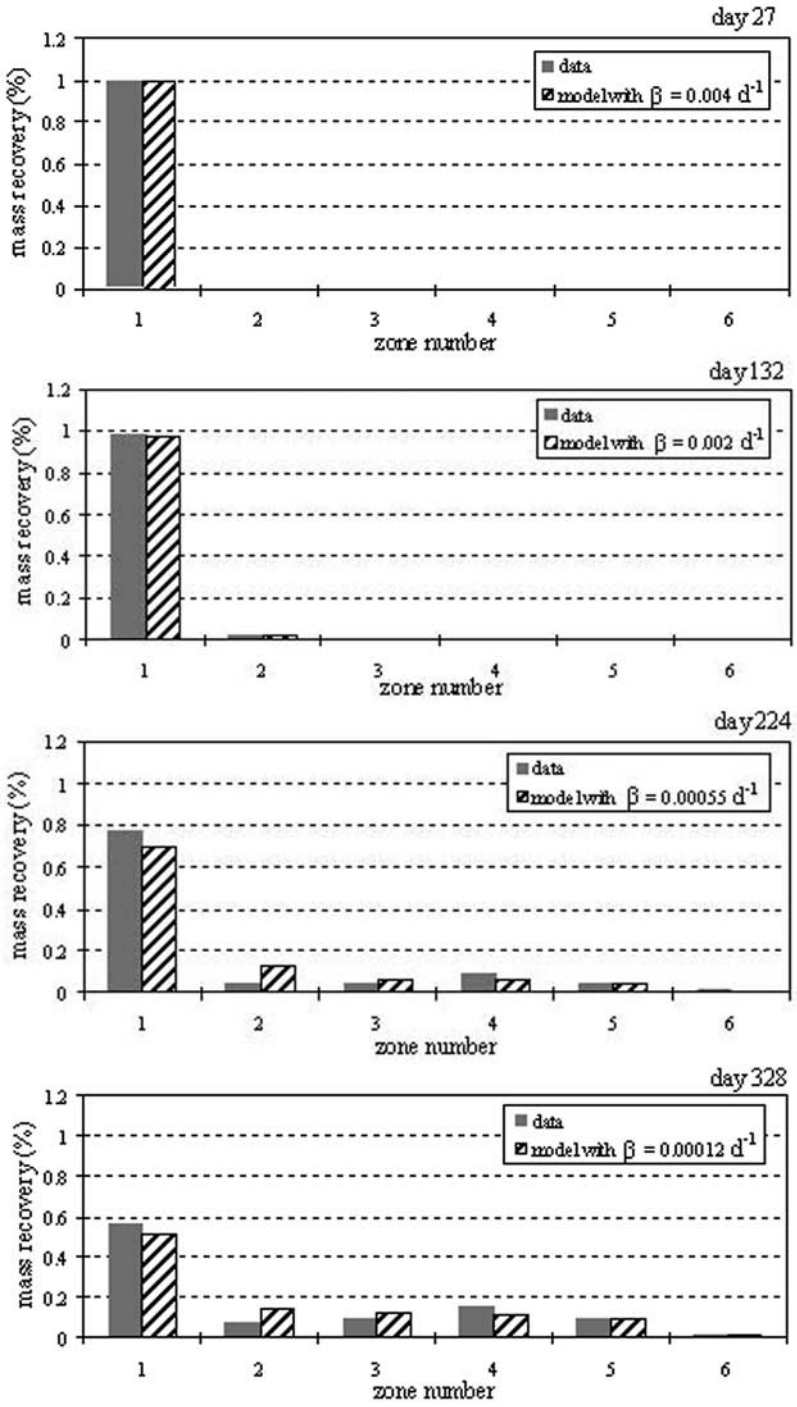

Figure 11. Simulated mass with trapping (single porosity assumption) in each of zones 1 through 6 (50 m width) compared to data from each snapshot.

fourth is decreased by a factor of 2.4. Essentially, the β values had to change to compensate for the changed flow field and its effect on the movement of the center of mass. The logic of this can be seen by examining Figure 8. In a rough sense, the single average head difference was higher during the first half of the experiment than that used previously, so β had to increase to slow down the mass center advance. During the second half the average gradient was lower, so β had to decrease to speed up the mass center advance. This simply shows that all approximations used in a model or conceptual errors made in deriving a model, will have an effect on calibrated parameters.

7. Causes of Scale-Dependency

[42] As shown in Tables 5 and 6, the mass transfer rate coefficient β decreases with time and with the scale of the evolving plume. This scale-dependence behavior may be attributed to (1) multirate diffusion processes occurring in a

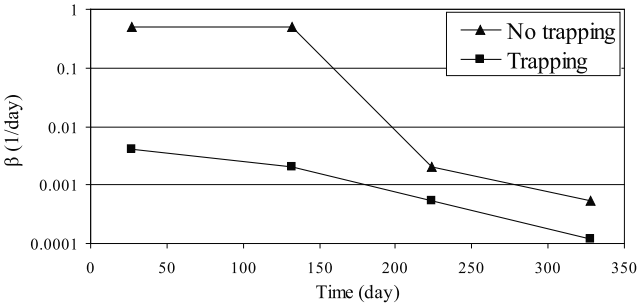

Figure 12. Semi-log plot showing the calibrated scale-dependence of the mass transfer coefficient "β" as a function of time. The simulation based on the calibrated β with trapping near the source reproduces both the observed plume mass center versus time and the observed mass balance corrected for radioactive decay of the tritium tracer.

highly heterogeneous system, and (2) limitations of the first-order approximation of mass transfer between mobile and immobile regions. We focus our discussion here on the limitations of the first-order mass transfer approximation and its effect on scale dependence of the β value, by comparing first-order results fitted to an analytical solution [*Moridis*, 1999].

[43] In a dual-porosity model with equation (2), the mass transfer rate [*Feehley et al.*, 2000] is assumed to be proportional to the difference in the average concentrations between the mobile and immobile regions of each grid block. This assumption is equivalent to the assumption of a linear change of immobile concentration from the edge to the center of the immobile region. At the pore scale, the simulation time step size is approximately on the same timescale as that of diffusion equilibrium—e.g., at the pore scale of fine gravel, with a radius of $l = 2$ mm, the timescale (t_{eq}) for equilibrium is $t_{eq} = 0.41l^2/D_m = 0.19$ days for the medium's diffusion coefficient $D_m = 1.0 \times 10^{-10}$ m^2/s [*Crank*, 1975, p92]. This small timescale indicates that in each numerical-simulation time step, the mobile and immobile pore fractions are in equilibrium, and there is no need to use the dual-porosity model for treating the pore-scale heterogeneity in diffusion. At the tens-of-centimeter scale (similar to the vertical gridblock size of 0.5 m), the above assumption for the immobile fraction of a gridblock may not be applicable. The most significant manifestation of the strong heterogeneity at the MADE site is that centimeter-thick, high-permeability, fast-flow paths (mobile regions) are in contact with tens-of-centimeter-thick, low-permeability, low-flow regions (immobile regions), as evident from detailed measurements of hydraulic conductivity [*Rehfeldt et al.*, 1992; *Boggs et al.*, 1993] and more theoretical considerations [*Zheng and Gorelick*, 2003]. In this case, the diffusive mass transfer plays a key role in retarding the limited tritium mass initially released in the fast-flow paths, as shown in section 6. In the thin fast-flow paths, the solution can be assumed to be well mixed, because of the relatively small thickness of the flow paths and the large hydrodynamic dispersion (including diffusion). However, the transient diffusive penetration into the thick, immobile regions takes a long time to satisfy the above assumption. This relatively large timescale for diffusion may result in a significant approximate error in the first-order mass transfer model. As a result, the limitations of this first-order approximation may (at least partially) contribute to the time-dependence of the calibrated β values observed in section 6.

[44] To quantify the effect of the first-order approximation on the calibrated β values, we employed a semi-analytical solution for a one-dimensional closed system under fully saturated conditions. This system consists of a high-permeability layer of thickness d_m and an underlying low-permeability layer of thickness d_{im}, with a total porous-medium volume of V ($\equiv (d_{im} + d_m)A$) and a mobile-immobile interface area of A. Note that d_m and d_{im} respectively are the half thickness of mobile and immobile regions when applied to a geologic site. The mobile region is assumed to be well-mixed over time. Initially, the mobile region contains a unit-concentration solute, whereas the immobile region is solute-free. Under such conditions, the transient diffusive penetration of solute and the redistribution of the total solute mass in the mobile and immobile regions can be investigated using the semi-analytic solution developed by *Moridis* [1999] for analyzing laboratory diffusion-cell tests. To assure that the fractional mobile porosity is consistent with that used in previous sections, we used $d_{im} = 7d_m$, assuming that the total porosity for the mobile and immobile regions are the same at the local scale. The model parameters used are: mobile and immobile (total) porosity $\theta = 0.35$, a tritium diffusion coefficient in free water of $D_w = 2.0 \times 10^{-9}$ m^2/s, and a tortuosity factor of $\tau = 0.2$, leading to the immobile medium's diffusion coefficient of $D_{im} = \tau D_w = 4 \times 10^{-10}$ m^2/s. In the first case, we used $d_{im} = 0.14$ m. The solute concentration profiles at 1, 27, 132, 224, 328 days are shown in Figure 13a. At 27 days, the system has not reached equilibrium, with a penetration depth of about 0.1 m. At 132 days, the system is at quasi-equilibrium, and the solute concentrations in the mobile and immobile regions are close. At the two later times (224 and 328 days), the system is almost at equilibrium. As shown in Figure 13b, with the increase in the thickness of the low-permeability layer to $d_{im} = 0.35$ m, it takes longer for the system to reach equilibrium. In this case, the system has not reached equilibrium at the latest time of 328 days.

Table 6. The Calibrated β Values Resulting From the Case With Trapping, but Applying a Single Average Head Gradient to the Problem Instead of the 3 Different Gradients Listed in Table 2[a]

Snapshot Time (d)	27	132	224	328
Mass Center (m): (data)	3.9	8.1	46.5	76.8
Mass Center (m): (Model)	4.0	8.6	46.9	76.6
	$\beta = 0.008$d^{-1}	$\beta = 0.006$d^{-1}	$\beta = 0.0002$d^{-1}	$\beta = 0.00005$d^{-1}

[a]It is evident that different approximations to the overall gradient also affect the calibrated mass transfer rate coefficients.

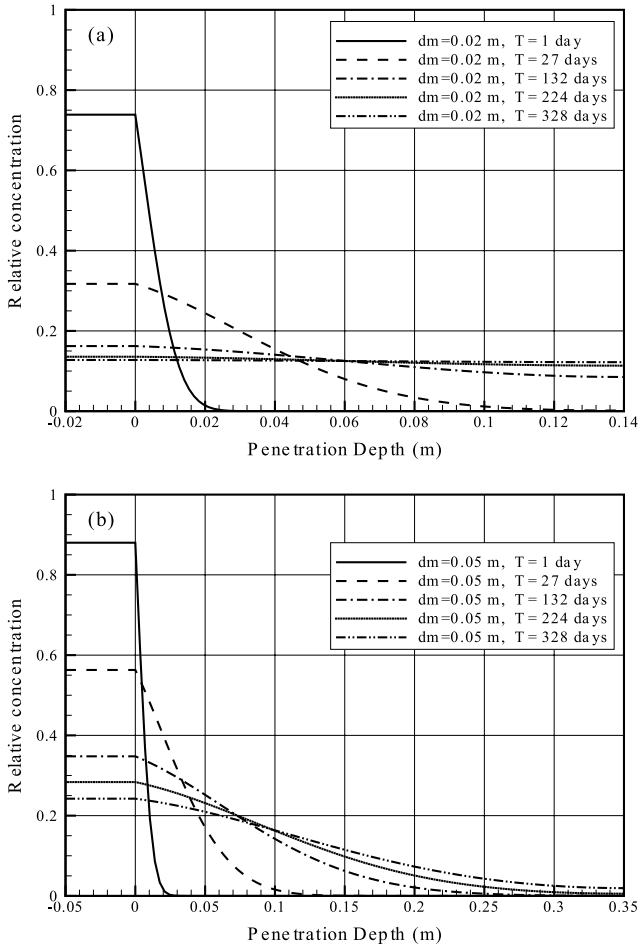

Figure 13. Redistribution of tritium mass initially injected in the mobile region caused by pure diffusive mass transfer between the mobile and immobile regions in the case of mobile region of (a) 0.02 m thick, and (b) 0.05 m thick.

[45] On the basis of the analytical solution at different times, we calculated the apparent mass transfer rate coefficient "β" value averaged over each of the five time intervals between 0 and 328 days. For the one-dimensional closed system, concentrations in the mobile and immobile regions used in the dual-porosity model depend only on the time since tritium was injected. For a time interval (t_1, t_2), equation (2) can be rewritten in the integral form:

$$\int_V \int_{t_1}^{t_2} \theta_{im} dC_{im}(t) dV = \int_V \int_{t_1}^{t_2} \beta(t)[C_m(t) - C_{im}(t)] dt dV \quad (12a)$$

with

$$\theta_{im} = \frac{d_{im}}{d_m + d_{im}}\theta. \quad (12b)$$

To calculate the average mass transfer coefficient, $\overline{\beta(t_1 \sim t_2)}$, for the time interval of interest, we rewrite equation (12a) in the finite difference form:

$$\overline{\beta(t_1 \sim t_2)} = \frac{\theta_{im}[C_{im}(t_2) - C_{im}(t_1)]}{t_2 - t_1} \Big/ \frac{[C_m(t_1) - C_{im}(t_1)] + [C_m(t_2) - C_{im}(t_2)]}{2} \quad (12c)$$

The average mass transfer coefficient is calculated using the exact concentrations for the mobile region: $C_m(t_1)$ and $C_m(t_2)$ obtained through the semi-analytic solution. The concentrations in the immobile region are calculated using the mass balance equation:

$$C_{im}(t_i) = [1 - C_m(t_i)]d_m/d_{im}, \quad (12d)$$

where t_i (i = 1, 2) are the start and end of the time interval.

[46] The average concentrations ($C_{im}(t_1)$ and $C_{im}(t_2)$) in the immobile region are calculated by assuming the same well-mixing as in the dual-porosity model, and the total solute mass lost into the immobile region by diffusion is known from $\Delta M = \theta d_m A[C_m(t_1) - C_m(t_2)]$. The concentration difference between the mobile and immobile regions is calculated for each observation time, with the averaged concentration difference for a time interval calculated using the concentration-difference values at the two observation times of this interval. The average mass transfer rate coefficient for each interval is calculated using equation (12c). Note that equations (12) are based on the fractional splitting of mobile and immobile regions which are assumed to be two overlapping continua used in the dual-porosity model, whereas the closed system used in the analytic solution is represented by the two non-overlapping mobile and immobile regions. As a result, the immobile porosity (θ_{im} = 0.31) in equation (12b) is different from the total porosity (θ = 0.35) used for both mobile and immobile regions in the analytical solution.

[47] The calculated mass transfer rate coefficient is shown in Figure 14 as a function of time for the two cases of different mobile/immobile thickness. It is seen that the apparent mass transfer rate coefficient calculated from the exact analytic solution decreases with observation time, as discussed by *Zhou et al.* [2007, p176], even when the medium's diffusion coefficient is unchanged. This dependence of the β value on observation time stems from the fact that a sharp concentration gradient at the mobile-immobile interface at early time can only be captured in the first-order approximation by using a larger β value. At later time, the mobile and immobile regions reach quasi-equilibrium and the first-order approximation may be applicable, and the mass transfer rate coefficient might have a well-defined physical meaning.

[48] The physical value of the mass transfer rate coefficient used in equation (2) for the dual-porosity model may be calculated from the solute diffusion coefficient and geometric parameters of the mobile and immobile regions [e.g., *Haggerty and Gorelick*, 1995]. For a fractured rock, the diffusive mass transfer flux (q^A_{diff}) across a unit fracture-matrix interface area in a non-overlapping fracture-matrix system (for analytic solutions) is given by [*Zhou et al.*, 2006, 2007]:

$$q^A_{diff} = -\phi_{im} D_{im} \left.\frac{\partial C_{im}}{\partial z}\right|_{z=0} \quad (13a)$$

where ϕ_{im} is the total porosity of the rock matrix (i.e., immobile region in this study), D_{im} is the diffusion coefficient of the immobile region, and z is the coordinate perpendicular to the interface and positive into the immobile region from the interface at z = 0. For comparison with the

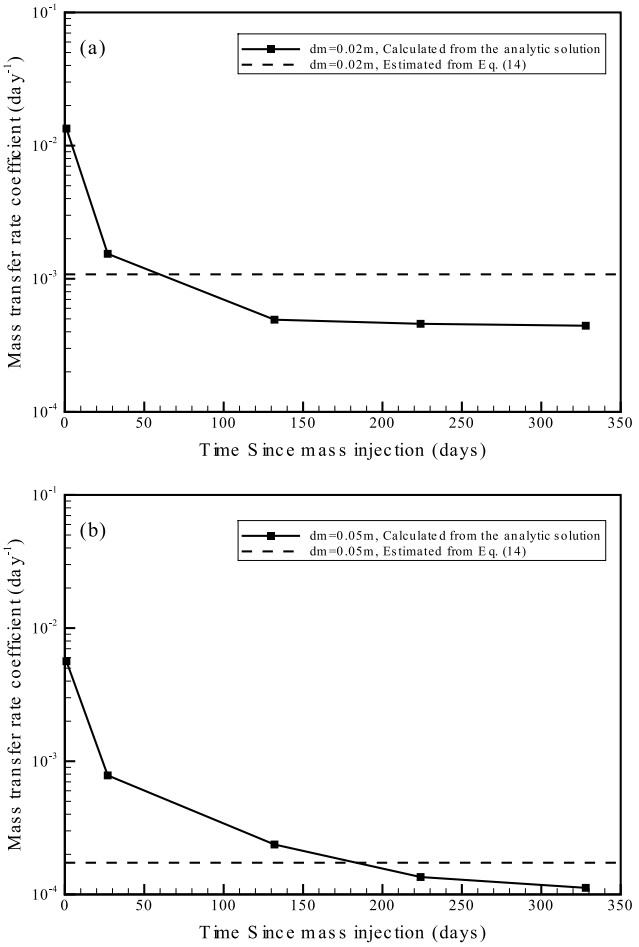

Figure 14. Calculated mass transfer rate coefficient values, as a function of time, from the simulated transient concentration-depth profiles in the case of mobile region of (a) 0.02 m thick, and (b) 0.05 m thick.

diffusive flux per unit volume of porous medium used in the dual-porosity model, we define the diffusive flux (q^V_{diff}) per unit volume of fractured rock for the closed system:

$$q^V_{diff} = -\phi_{im} D_{im} \left.\frac{\partial C_{im}}{\partial z}\right|_{z=0} \frac{A}{V} = -\frac{\phi_{im} D_{im}}{d_m + d_{im}} \left.\frac{\partial C_{im}}{\partial z}\right|_{z=0} \approx -\frac{\phi_{im} D_{im}}{(d_m + d_{im}) F d_{im}} (C_m - C_{im}) \quad (13b)$$

where F is the fractional thickness of the immobile region used to calculate the concentration gradient. For example, as commonly done with the dual-porosity model, the center of the immobile region is used, leading to $F = 0.5$. Considering that the left-hand term in equation (2) is also the diffusive flux through the mobile-immobile interface per unit volume of porous medium, we compare equation (2) to equation (13b), and, through further manipulation, derive an expression for the mass transfer rate coefficient given by:

$$\beta = \frac{\phi_{im} D_{im}}{F(d_m + d_{im}) d_{im}} = \frac{1}{F} \theta_{im} \frac{D_{im}}{d^2_{im}}. \quad (14)$$

[49] At quasi-equilibrium, the first-order approximation is valid, and the physical β value depends only on the diffusion coefficient, immobile porosity, and the thickness of the immobile regions. The physical β values calculated for the two different d_m values using $F = 0.5$ are also shown in Figure 14.

[50] The physical meaning of the mass transfer coefficient used in the dual-porosity model in equation (14) is consistent with that used in the multirate model [*Haggerty and Gorelick*, 1995]. In the multirate model, the mass transfer rate coefficient β values used in equation (1) are defined as:

$$\beta_j = \frac{1}{F_j} \theta_{im} D_{im} / l^2, \qquad j = 1, 2, \ldots, N \quad (15)$$

where l is the length of the diffusion pathway within a rock matrix or a pore [*Haggerty and Gorelick*, 1995; *Haggerty et al.*, 2001]. Note that in equation (15) the mass transfer rate coefficient is related to the immobile porosity because of their definition in equation (1), whereas in the original references of the multirate diffusion model [e.g., *Haggerty and Gorelick*, 1995], the mass transfer-rate coefficient is defined by $\alpha_j = \frac{1}{F_j} D_{im} / l^2$. The F_j values in the multirate model are in a numerical series equivalent to the diffusion model [*Haggerty and Gorelick*, 1995, Table 1]. In the standard first-order approximation of the multirate model for the dual-porosity model, $F = 1/3$, whereas the late-time approximation uses $F = 4/\pi^2$ [*Haggerty and Gorelick*, 1995, equation (26) and Table 1].

[51] Fundamentally, equations (14) and (15) are identical in that the diffusion rate coefficient is related to the inverse square of the diffusion length. In the multirate diffusion model, a probability distribution of the diffusion rate coefficient can be used to represent both the transient diffusion penetration into a solute-free immobile region, using analytical solutions [*Haggerty and Gorelick*, 1995], and heterogeneous diffusion caused by differently sized pores and variable thickness of the immobile clay layers in porous media [*Haggerty et al.*, 2000]. The multirate model implicitly captures the temporal scale-dependency behavior of the mass transfer coefficient caused by the transient penetration of diffusion into individual pores or layers, by using the multirate series in equation (15). In this case, the diffusion coefficient D_{im} is constant. However, this key parameter for diffusive transport exhibits strong heterogeneity, depending on heterogeneous porosity and formation factors, as evidenced by recent studies involving imaging techniques [e.g., *Altman et al.*, 2004]. The scale dependency of the mass transfer coefficient caused by the heterogeneity of the diffusion coefficient may also be interesting, but beyond the scope of discussion in this section. The reader may be referred to *Haggerty et al.* [2004] for the lumped scale-dependence of the mass transfer rate coefficient observed in the field, and to *Zhou et al.* [2007] for the scale dependence of the field-scale, effective matrix diffusion coefficient for fractured rock.

[52] Naturally, contaminants and solutes migrate through fast-flow paths (or fractures), with diffusive loss into immobile regions (rock matrix), and with limited contaminant/solute mass. When the thickness of the mobile region is much larger than that of immobile regions, the fractional

mass loss caused by diffusion into immobile regions may be negligible—in which case, the advection-dispersion equation is more applicable. When the mobile region is much thinner than the immobile region, the fractional mass loss by diffusion may be significant. As a result, diffusive transport must be included in numerical simulations. A good example for the latter is the MADE site, where the major manifestation of heterogeneity is that thin fast-flow paths are imbedded into low-permeability lenses, all of complicated geometry. This leads to diffusive transport being one of the dominant transport processes. Of course, natural heterogeneity is much more complicated than the special cases considered here, leading to a highly complex situation and many factors, often advective in nature, contributing simultaneously to the scale-dependency of β. (This degree of complexity is the main motivation for using the simple first order mass transfer rate expression as a practical alternative.) Nevertheless, the β scale-dependency calculated for the MADE-2 experiment may be reduced through the use of a 3-D transport model that simulates gradients driving diffusion in some more direct manner.

8. Discussion and Conclusions

[53] Using a dual-porosity or dual-domain transport model, a more complete analysis of the MADE-2 experiment, compared to analyses developed previously, has been presented. Results show that a single mass transfer rate coefficient will be scale-dependent, and decreasing with time. For the particular data studied, a near-exponential decrease with time was observed. It was also shown that use of an approximate first-order mass transfer rate expression, rather than an expression using transient concentration gradients to drive diffusion-limited mass transfer between mobile and immobile regions, undoubtedly contributes to the observed scale-dependent behavior. This type of scale-dependency (mass transfer rate coefficients decreasing with time) is in agreement with that observed previously in most heterogeneous sediments [*Haggerty et al.*, 2004]. However, studies in fractured rock show that the matrix diffusion coefficient, similar but not mathematically analogous to the mass transfer rate coefficient, increases with time or mean travel distance, as discussed by *Liu et al.* [2004b, 2007] and *Zhou et al.* [2006, 2007].

[54] In order to develop a self-consistent, dual-porosity model, it was necessary to assume that the injected tritium tracer was trapped hydraulically in the vicinity of the injection site, and we offer this assumption as a hypothesis that requires experimental verification. Simple observation of the tracer plume that developed in the field strongly suggests trapping near the source, but evidently the trapping mechanism was not captured by the many K measurements based on the borehole flowmeter. Possibly this could be due to the geometry of smaller-scale low K sediments not being resolved by the flowmeter tests, which produce a 360 degree average at each measurement location. If both higher and very low K sediments exist in different portions of a measurement zone, then the low K sediments will be averaged away.

[55] Trapping was simulated by lowering all K values in the vicinity of the injection site by a factor of 30, while holding all other K values at their measured or measurement-interpolated values. Resulting simulations were able to reasonably match the movement of the center of mass as observed in the field and also the observed and anomalous mass recovery ratios at each snapshot. Overall plume geometry was reasonable also. It is highly unlikely that this simple lowering of K values captured the actual pattern of heterogeneity that led to the trapping, but apparently it did approximate the overall effect on plume development. Other patterns of K lowering might work just as well, or even better, but this possibility was not explored.

[56] It was further shown that calibrated mass transfer rate coefficients are not unique in the absence of a perfect model. Different K interpolations, model and boundary condition approximations, mass transfer rate expressions and conceptual errors in model development will lead to different degrees of scale-dependency. (This is also true when dispersivity is used as a calibration parameter.) Nevertheless, the dual-porosity model and its possible generalizations are conceptually simple, relatively easy to apply mathematically and they deal with differences in advection that are probably the root cause of dispersion in natural heterogeneous sediments. Also, a small, more realistic amount of local hydrodynamic dispersion is not precluded.

[57] The multiporosity conceptualization of mass transport in natural porous media provides a window into the inherent complexity of the transport process. Evidently, at the Darcy scale a unique value of concentration does not exist at each point. There will be as many concentration values as there are porosities. This non-uniqueness of concentration for the MADE sediments was also shown directly by the experiments of *Boggs and Adams* [1992].

References

Adams, E. E., and L. W. Gelhar (1992), Field study of dispersion in a heterogeneous aquifer, 2. Spatial moments analysis, *Water Resour. Res.*, *28*(12), 3293–3307.

Altman, S. J., M. Uchida, V. C. Tidwell, C. M. Boney, and B. P. Chambers (2004), Use of X-ray absorption imaging to examine heterogeneous diffusion in fractured crystalline rocks, *J. Contam. Hydrol.*, *69*, 1–26.

Barlebo, H. C., M. C. Hill, and D. Rosbjerg (2004), Investigating the Macrodispersion Experiment (MADE) site in Columbus, Mississippi, using a three-dimensional inverse flow and transport model, *Water Resour. Res.*, *40*, W04211, doi:10.1029/2002WR001935.

Benson, D. A., A. R. Schumer, M. M. Meerschaert, and S. W. Wheatcraft (2001), Fractional dispersion, Levy motion, and the MADE tracer tests, *Transp. Porous Media*, *42*, 211–240.

Berkowitz, B., and H. Scher (1998), Theory of anomalous chemical transport in random fracture networks, *Phys. Rev. E*, *57*, 5858–5869.

Boggs, J. M., and E. E. Adams (1992), Field study of dispersion in a heterogeneous aquifer 4: Investigation of adsorption and sampling bias, *Water Resour. Res.*, *28*(12), 3325–3336.

Boggs, J. M., S. C. Young, L. M. Beard, L. W. Gelhar, K. R. Rehfeldt, and E. E. Adams (1992), Field study of dispersion in a heterogeneous aquifer 1. Overview and site description, *Water Resour. Res.*, *28*, 3281–3291.

Boggs, J. M., L. M. Beard, and W. R. Waldrop (1993), Transport of tritium and four organic compounds during a natural-gradient experiment (MADE-2), *Electric Power Research Institute*, Palo Alto, California.

Coats, K. H., and B. D. Smith (1964), Dead-end pore volume and dispersion in porous media, *Soc. Pet. Eng.*, *4*, 73–84.

Crank, J. (1975), *The Mathematics of Diffusion*, 2nd ed., Oxford Univ. Press, New York.

Feehley, C. E. (1999), A dual-domain mass transfer approach for modeling solute transport in heterogeneous aquifers: An application to the MADE site, M. S. Thesis, University of Alabama, Tuscaloosa, AL.

Feehley, C. E., C. Zheng, and F. J. Molz (2000), A dual-domain mass transfer approach for modeling solute transport in heterogeneous aquifers: Application to the Macrodispersion Experiment (MADE) site, *Water Resour. Res.*, *36*, 2501–2515.

Flach, G. P., S. A. Crisman, and F. J. Molz (2004), Comparison of single-domain and dual-domain subsurface transport models, *Ground Water*, *42*, 815–828.

Guan, J. (2006), Analysis of a 3-D tritium transport experiment at the MADE site, Ph.D. Dissertation, Clemson University, Clemson, SC.

Haggerty, R., and S. M. Gorelick (1995), Multiple-rate mass transfer for modeling diffusion and surface reactions in media with pore-scale heterogeneity, *Water Resour. Res.*, *31*, 2383–2400.

Haggerty, R., S. A. McKenna, and L. C. Meigs (2000), On the late-time behavior of tracer test breakthrough curves, *Water Resour. Res.*, *36*(12), 3467–3479.

Haggerty, R., S. W. Fleming, L. C. Meigs, and S. A. McKenna (2001), Tracer tests in a fractured dolomite 2. Analysis of mass transfer in single-well injection-withdrawal tests, *Water Resour. Res.*, *37*, 1129–1142.

Haggerty, R., C. F. Harvey, C. F. V. Schwerin, and L. C. Meigs (2004), What controls the apparent timescale of solute mass transfer in aquifers and soils? A comparison of experimental results, *Water Resour. Res.*, *40*, W01510, doi:10.1029/2002WR001716.

Harvey, C. F., and S. M. Gorelick (2000), Rate-limited mass transfer or macrodispersion: Which dominates plume evolution at the Macrodispersion Experiment (MADE) site?, *Water Resour. Res.*, *36*, 637–650.

Hill, M. C., H. C. Barlebo, and D. Rosbjerg (2006), Reply to comment by F. Molz et al. on ''Investigating the Macrodispersion Experiment (MADE) site in Columbus, Mississippi, using a three-dimensional inverse flow and transport model'', *Water Resour. Res.*, *42*, W06604, doi:10.1029/2003WR004624.

Liu, G., C. Zheng, and S. M. Gorelick (2004a), Limits of applicability of the advection-dispersion model in aquifers containing connected high-conductivity channels, *Water Resour. Res.*, *40*, W08308, doi:10.1029/2003WR002735.

Liu, H. H., G. S. Bodvarsson, and G. Zhang (2004b), Scale dependency of the effective matrix diffusion coefficient, *Vadose Zone Journal*, *3*, 312–315.

Liu, H. H., Y. Zhang, Q. Zhou, and F. J. Molz (2007), An interpretation of potential scale dependence of the effective matrix diffusion coefficient, *J. Contam. Hydrol.*, *90*, 41–57.

McDonald, M. G., and A. W. Harbaugh (1988), A modular three-dimensional finite-difference ground-water flow model: U. S. Geological Survey Techniques of Water-Resources Investigations, Chapter 6-A1, 586.

Molz, F. J., and G. K. Boman (1993), A stochastic interpolation scheme in subsurface hydrology, *Water Resour. Res.*, *29*, 3769–3774.

Molz, F. J., H. H. Liu, and J. Szulga (1997), Fractional Brownian motion and fractional Gaussian noise in subsurface hydrology: A review, presentation of fundamental properties, and extensions, *Water Resour. Res.*, *33*, 2273–2286.

Molz, F. J., C. Zheng, S. M. Gorelick, and C. F. Harvey (2006), Comment on ''Investigating the Macrodispersion Experiment (MADE) site in Columbus, Mississippi, using a three-dimensional inverse flow and transport model'' by Heidi Christiansen Barlebo, Mary C. Hill and Dan Rosbjerg, *Water Resour. Res.*, *42*, W06603, doi:10.1029/2005WR004265.

Moridis, G. (1999), Semianalytical solutions for parameter estimation in diffusion cell experiments, *Water Resour. Res.*, *35*, 1729–1740.

Rehfeldt, K. R., J. M. Boggs, and L. W. Gelhar (1992), Field study of dispersion in a heterogeneous aquifer 3. Geostatistical analysis of hydraulic conductivity, *Water Resour. Res.*, *28*, 3309–3324.

Warren, J. E., and P. J. Root (1963), The behavior of naturally fractured reservoirs, *Society of Petroleum Engineers Journal, 3,* 245–255, WSRC-TR-2002-00291, Rev. 1, Dual-Media Contaminant Transport Models 45.

Weast, R. C. (Ed.) (1972), *Handbook of Chemistry and Physics,* 52nd Edition, The Chemical Rubber Company, Cleveland, OH 44128.

Zheng, C., and S. M. Gorelick (2003), Analysis of the effect of decimeter-scale preferential flow paths on solute transport, *Ground Water*, *41*, 142–155.

Zheng, C., and P. P. Wang (1999), MT3DMS; A modular three-dimensional multispecies transport model for simulation of advection, dispersion and chemical reactions of contaminants in groundwater systems (Release DoD_3.50.A); Documentation and user's guide, U.S. Army Corps of Engineers, SERDP-99-June 1998.

Zhou, Q., H. H. Liu, G. S. Bodvarsson, and F. J. Molz (2006), Evidence of multi-process matrix diffusion in a single fracture from a field tracer test, *Transp. Porous Media*, *63*, 473–487, doi:10.1007/s11242-005-1123-9.

Zhou, Q., H. H. Liu, F. J. Molz, Y. Zhang, and G. S. Bodvarsson (2007), Field-scale effective matrix diffusion coefficient for fractured rock: Results from literature survey, *J. Contam. Hydrol.*, *93*, 161–187, doi:10.1016/j.jconhyd. 2007. 02.002.

J. Guan, Daniel B. Stephens & Associates, Inc., Albuquerque, NM 87111, USA.

H. H. Liu and Q. Zhou, Earth Sciences Division, Lawrence Berkeley National Laboratory, University of California, Berkeley, CA 94720, USA.

F. J. Molz, Department of Environmental Engineering and Earth Science, Clemson University, Anderson, SC 29625, USA. (fredi@clemson.edu)

C. Zheng, Department of Geological Sciences, University of Alabama, Tuscaloosa, AL 35487, USA.